Bandwidth Enhancement of Five-port Reflectometer Using ENG DSRR Metamaterial for Microwave Imaging Application

Toufiq M. Hossain[1, *], Mohd F. Jamlos[1, *], Mohd A. Jamlos[2, 3],
Samir S. Al-Bawri[2, 4], Sathish Sugumaran[5], and Fatimah Dzaharudin[1]

Abstract—A five-Port Reflectometer (FPR) with the integration of ultra-wideband (UWB) Epsilon Negative (ENG) Double Split Ring Resonator (DSRR) metamaterial array is introduced in this paper for microwave imaging (MWI) application. The designed DSRR with consists of two concentric rings with a split in each which are spatially rotated by 180°, formed an inverted structure to exhibit a wide negative epsilon bandwidth of 187% (from 0.5 GHz to 15 GHz). The FPR is designed using a ring junction topology and semi-circularly curved inter-port transmission lines (TLs) which are placed between five equally spaced ports. Localizing the DSRR metamaterial in a periodic array of 5×4 at the ground plane of FPR lead to 79.79% fractional bandwidth compared to only 42.65% without metamaterial and improved the reflection coefficient within the operating frequencies of 0.991 GHz to 2.2576 GHz. Equivalent circuit model has been alluded with an intricate description of different array configurations of the metamaterial unit cell. Comparison of EM simulation and circuit simulation has been performed to validate the equivalent circuit model. It is found that the existence of stray capacitance, C_{stray} which is represented by the DSRR configurations, significantly influenced the resonant frequency and bandwidth of FPR. Measured results of the proposed design suits well with the simulations and prove higher efficacious applicability of the proposed design for microwave imaging application. A comparison of the reconstructed image also proves its superiority with respect to non-metamaterial-based counterpart.

1. INTRODUCTION

Microwave imaging (MWI) has gained lot of attention in recent days for cancer detection research [1–8]. It has proved its efficacy as an alternative medical screening especially in breast, lung and brain tumor detection due to its non-invasive, non-ionizing and cost effective feature which allow frequent examination and portability [1–3]. The main basis of MWI is based on the dielectric contrast between tumorous tissues and healthy tissues [4, 5]. The early detection is considered to be very important in cancer diagnosis to ensure a better treatment which can be materialized by using portable devices for MWI with high detection feature [2, 6–8]. However, use of expensive Vector Network Analyzers (VNAs) [4, 7, 9] retards the portability of MWI system and therefore researchers have suggested alternative devices for the transmission and reception of the signals in the imaging process. FPRhas been favored over VNA as suitable alternative in microwave imaging [10]. Moreover, FPR does not require reference power detector, enabling faster and cost effective measurements [11]. A broader bandwidth of FPR is a requirement to equip an efficacious microwave imaging system. Due to the theoretical characteristic impedance and length restraints of inter-port transmission lines, single-ring-based five-port reflectometer (otherwise called fundamental FPR) has a narrow operational bandwidth [12]. Different

approaches have been adopted by the researchers including double-ring-based design [12] and multi-matching-section-based design with [13] and without [10, 12] tapered transmission line to enhance the bandwidth of single-ring-based FPR proposed by Riblet et al. and others [14–19]. However these designs are bigger in size [19]. In [19], superstrate-based approach has been carried out to enhance the fractional bandwidth. However, this is at the cost of fabrication complexity. To the best of authors' knowledge, no research has been carried out to implement metamaterial unit cells to enhance the fractional bandwidth of FPR. The necessity of higher image resolution is dependent on the broader bandwidth of the FPR to be involved in the imaging system as mentioned earlier. Among different ways of bandwidth enhancement, metamaterials (MTMs) have gained much popularity in recent days.

MTMs are artificial homogeneous periodic structures with properties and behaviors which are impossible to elicit from naturally-occurring materials, such as negative permittivity, negative permeability,

negative refractive index and backward propagation [20, 21]. Epsilon negative (ENG) and mu negative (MNG) metamaterials are categorized depending on the characteristics of permittivity (epsilon) and permeability (mu) to be negative. As the electric and magnetic characteristics of MTMs extending beyond nature, they have been used for versatile applications covering cloaking, lens, SAR reduction, bandwidth enhancement, gain enhancement and antenna miniaturizations, and multiband applications [20]. Among the variety of shapes of MTMs, split ring resonator (SRR) or otherwise called as dual split ring resonator (DSRR) is one of the simplest designs, showing negative indexed behavior. The theory and electromagnetic analysis of the structures are established through copious researches. Structures based on or derived from generic SRRs have been used in sensors for DNA hybridization and dielectric sensing [22]. Different SRR have been reported with epsilon negative characteristics. Circular SRR (DSRR)-based composite structures in [21] has shown a fractional bandwidth with negative permittivity, $BW_{ENG} = 10\%$ covering approximately a region of 500 MHz in the microwave regime (4.7 GHz to 5.2 GHz). Inspiring from the other applications of DSRR structures, researchers have used this structure for UWB and microwave imaging applications using circular, rectangular and octagonal SRR-based UWB antennas as presented in [23–25] respectively. The overall frequency zones with VSWR < 2 are expanding 3.4–12.5 GHz [23], 3.1–15 GHz [24] and 5.2–13.9 GHz [25]. In [23], the metamaterial has shown three zones with ENG characteristics, namely 5.3 GHz to 6 GHz, 7.27 GHz to 7.37 GHz, 10.31 GHz to 13.26 GHz. However, the highest fractional bandwidth with negative permittivity, BW_{ENG} of this literature is 25.032%, shown by the third zone (10.31 GHz to 13.26 GHz). With regards to the rectangular SRR presented in [24], four zones showed negative permittivity such as, 3 GHz to 5.27 GHz, 8.42 GHz to 9.96 GHz, 12.56 GHz to 13.90 GHz, 14.11 GHz to 15 GHz and highest fractional bandwidth, BW_{ENG} is 54.9% for the first band. The highest value of BW_{ENG} is 63.63% for the second type of the designs presented in [25]. In [26], rectangular SRR shaped metamaterial in conjunction with capacitive loaded strips (CLS) have been used for designing a UWB antenna. However, the epsilon negative characteristics are not presented in that work.

Double split ring resonator (DSRR) has potential to the enhance bandwidth of antenna and microwave circuit including reflectometer. Single ring FPR has a narrow fractional bandwidth which make them insufficient to be deployed for high accuracy microwave imaging. This manuscript intends to characterize the effects on the single FPR's bandwidth towards the microwave imaging resolution by existence or absence of ENG DSRR metamaterial array. The Proposed FPR as depicted in Figure 1, is designed to integrate with microwave imaging system. Among five ports, three ports will be connected with three power detectors (represented as PD1, PD2 and PD3 in Figure 1), while other two are connected to signal source and antenna. The measurement process will follow the procedure followed in [10] by transmitting microwave wave pulses through the antenna followed by processing the backscattered signal information by the processor along with the generation of image. The DSRR metamaterial consists of two concentric split rings. The splits in each of the rings are placed in 180° spatially inverted way, i.e., the splits in the rings are oppositely placed. The metamaterial array has been used at the ground plane of the proposed FPR. The proposed reflectometer operates within 0.5 GHz and 4 GHz, which is a commonly used band for microwave imaging, especially for brain imaging. Simulated and measured results are compared with theoretically designed primitive FPR. Equivalent circuit model of the FPR with and without DSRR metamaterial array have also been presented and elaborate description of the principle of operation is depicted using the description of the circuit model.
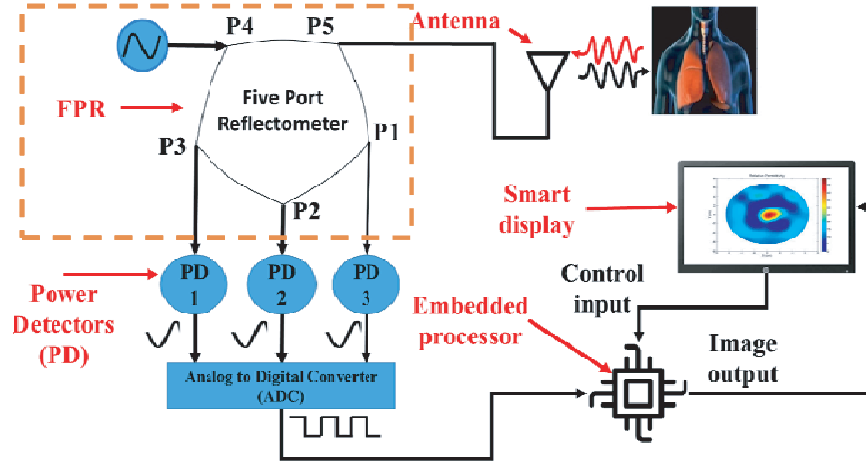
Figure 1. Diagramed portrayal of microwave imaging system with five port reflectometer.

The inclusion of metamaterial has increased the bandwidth of the FPR from 42.65% to 77.9%.

The manuscript is arranged in the following manner. Section 2 is related to the theory of five-port reflectometer. Section 3 deals with the design of ring junction five-port reflectometer followed by design of DSRR-based FPR. Section 4 describes the comparison results of FPR with and without ENG DSRR, and conclusions are drawn in Section 5.

2. THEORY OF FIVE-PORT REFLECTOMETER

Scattering-matrix element-eigenvalue relationship is used to determine the coupling characteristics of a symmetric FPR. These relationships are presented as follows [27]:

$$S_{11} = \frac{(S_1 + 2S_2 + 2S_3)}{5} \tag{1}$$

$$S_{12} = \frac{S_1 + 2S_2 \cos\left(\frac{2}{5}\right) + 2S_3 \cos\left(\frac{4}{5}\right)}{5} \tag{2}$$

$$S_{13} = \frac{S_1 + 2S_2 \cos\left(\frac{4}{5}\right) + 2S_3 \cos\frac{2}{5}}{5} \tag{3}$$

where S_j ($j = 1, 2, 3$) are the S-matrix eigenvalues demonstrating the eigen-reflection coefficients of port j. S_{jk} ($j, k = 1, 2, 3, 4, 5$) represents the S-matrix elements. The basic principal of 4-way equal power division in FPR is $S_{12} = S_{15}$, and $S_{13} = S_{14}$ (considering port 1). Due to reciprocity $S_{jk} = S_{kj}$. The properties of symmetric reciprocal FPR is determined using following conditions [17, 19, 27]:

$$|S_{11}| = 0 \tag{4}$$

$$|S_{12}| = |S_{13}| = 0.5 \tag{5}$$

$$\varphi S_{12} = \varphi S_{13} \pm \frac{2\pi}{3}(120°) \tag{6}$$

The reflection characteristics defined by (4) is referred as the figure of merit for the proper functioning of symmetric 5PR, as the coupling characteristics defined in (5) and (6) depend on the matching property of the FPR in (4).

3. METHODOLOGY

This section describes the design methodology of ring junction FPR at the first step. In second step the design and integration of ENG DSRR metamaterial at the ground plane of the designed ring junction FPR is discussed with fabrication and measurement process.

3.1. Design of Ring Junction FPR

Proposed FPR is designed using FR-4 substrate. The curved inter-port transmission line (TL) has an inter-port angular displacement $\alpha = 72° \left(= \frac{360°}{5}\right)$, confirming 4-way equal power division criterion defined in (4). The electrical length of the curved TL is represented as θ_{TL} while Y defines the normalized characteristic impedance of the curved inter-port TL (refer to Figure 2). Y_P is representing normalized characteristic impedance of the TL (with a width W_P) adjacent to each port. Equation (7) (as in Ref. [12, 19, 27]) provides the theoretical value of θ_{TL} and Y.

$$\theta_{\mathrm{TL}} = 0.211 \times \lambda_g, \quad Y = 1.12; \tag{7}$$

where λ_g represents guided wavelength (calculated using Equation (8) [19] for 1 GHz). The width of the inter-port TL (with width W_{TL} see Figure 2) and the TL (with width W_P) adjacent to each of the ports are calculated using *lineal* option available in Advanced Design System (ADS) software.
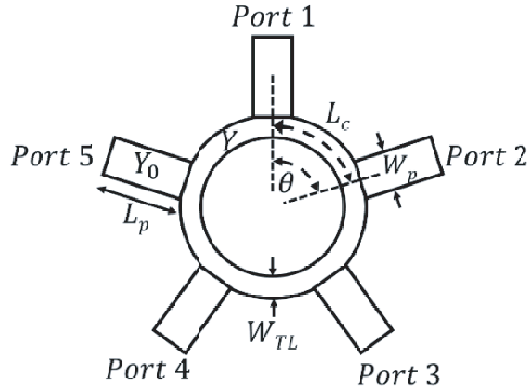

Figure 2. Proposed symmetric FPR.

The relationship between the width of the TL and the characteristic impedance can be shown as Equation (9) [28].

$$\lambda_g = \frac{c}{f\sqrt{\varepsilon_{\mathit{eff}}}} \tag{8}$$

$$Z_0 = \frac{60}{\sqrt{\varepsilon_{\mathit{eff}}}} \ln\left(8\left(\frac{t}{W}\right) + 0.25\left(\frac{W}{t}\right)\right) \tag{9}$$

where t represents the thickness of the substrate, W represents the width of the corresponding TL, and $\varepsilon_{\mathit{eff}}$ is the effective dielectric constant of the substrate given by Equation (10) [28] (ε_r is the relative

Table 1. Parametric description of proposed FPR.

Parameter	Dimension (mm)
W_{TL}	3.451620
W_p	2.8667
θ	$0.211 * \lambda_g$
ε_r	4.3
t	1.6
L_p	3
h	0.035
λ_g	158.8436

dielectric constant of the substrate (4.3 for FR-4)).

$$\varepsilon_{eff} = \frac{\varepsilon_r + 1}{2} + \frac{\varepsilon_r - 1}{2} \frac{1}{\sqrt{1 + 12t/W}} \tag{10}$$

The widths of the transmission lines are augmented to get specific impedance. The characteristic impedance of the port is $50\,\Omega$ for the TL adjacent to each port, i.e., TL with width W_P). The detail description of the parameters of the FPR is presented in Table 1.

3.2. Design of DSRR Metamaterial-based FPR

Figure 3(a) shows the design of proposed ENG DSRR unit cell consisting of two rings with $180°$ spatially placed slots. The width of the splits is denoted by a. The radius of the inner and outer ring is denoted by r_{in} and r_{out} respectively. The gap between two rings and the width of the rings are chosen to be same (denoted by b). The dimensions of the parameters of the DSRR metamaterial unit cell are presented in Table 2. The size of the proposed DSRR meta-atom is $0.01\lambda \times 0.01\lambda$, considering the wavelength corresponding to the lowest frequency of $0.5\,$GHz in the negative permittivity zone of the meta-atom. Perfect electric conductor (PEC) has been used as the boundary condition at the boundaries perpendicular to y-axis (denoted by green boundary) while perfect magnetic conductor (PMC) is set at boundaries perpendicular to x-axis (denoted by blue boundary) of designed DSRR unit cell, as shown in Figure 3(b). A plane wave propagation is allowed to be transmitted in $+z$-axis, which is confirmed using waveguide input and output ports along two remaining boundaries (denoted by red color in Figure 3(b)). The length of the outer ring of the unit cell is $2\pi r_{out} - a$ as opposed to the $2\pi r_{in} - a$ for the inner ring. Inner ring is introduced to have additional gap to boost capacitive effect which results in shifting frequency to the left as well as concentrating the electrical field into the gap. Proposed DSRR can be interpreted as a combination of inductor and capacitor. The gaps between rings, b act as capacitors and the metal rings exhibit properties of inductor depending on the length and width (b) of the rings [24]. The lengths of the rings and the gaps are optimized for the better negative permittivity of the structure as well as controlling the FPR characteristics. Figures 4(a) and (b) are representing
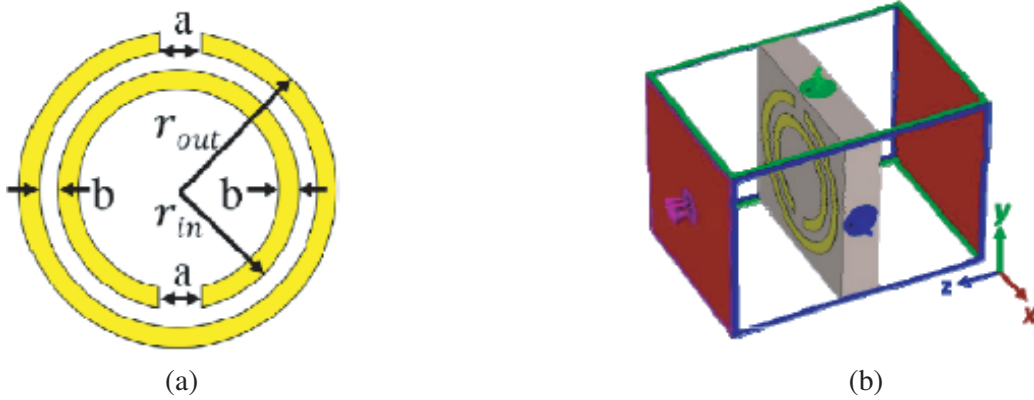

(a)   (b)

Figure 3. (a) Geometry of the meta-atom. (b) Simulation arrangement for the 1×1 array of the proposed DSRR meta-atom.

Table 2. Parametric depiction of the proposed DSRR meta-atom.

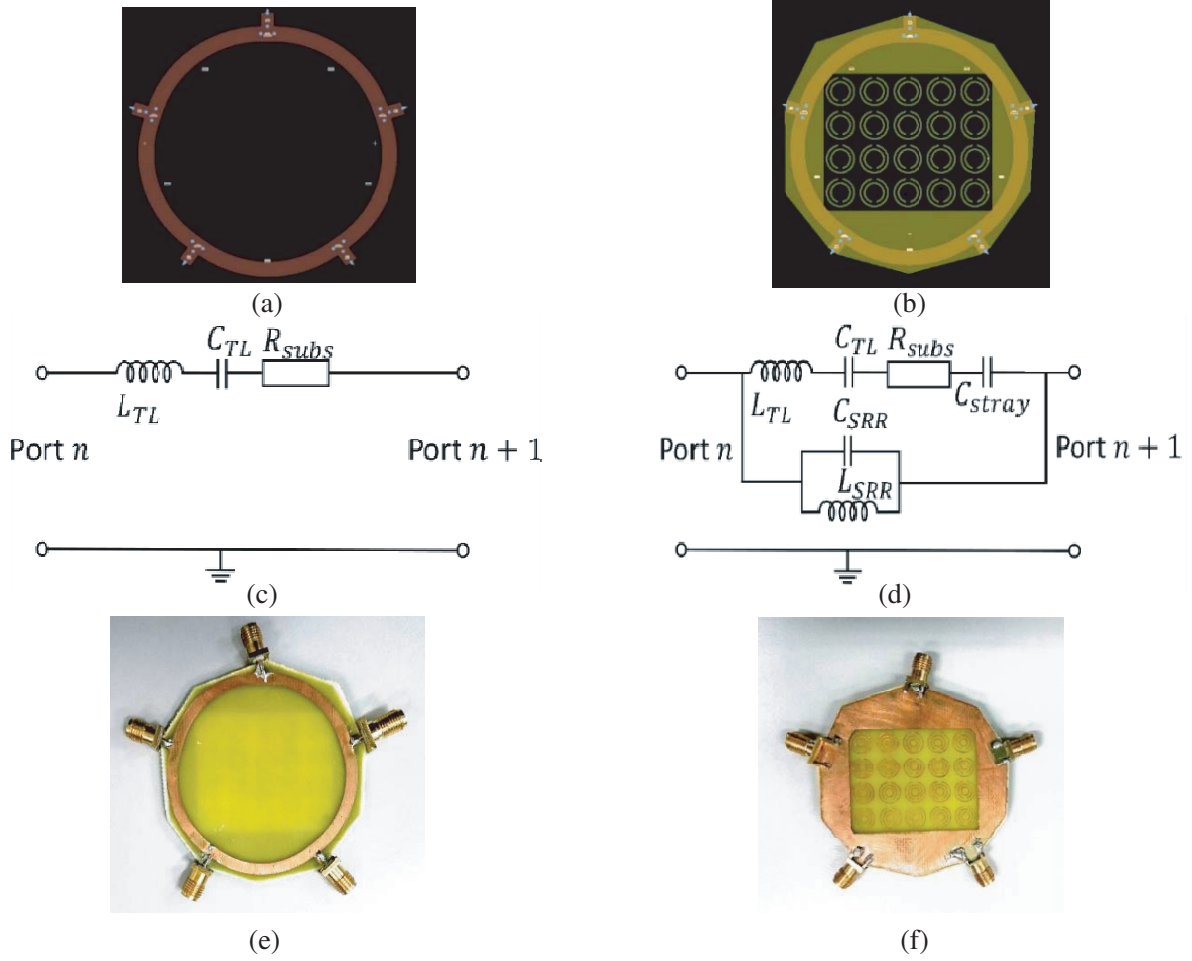| Parameter	Value (mm)
a	1
b	0.5
r_{in}	2.5
r_{out}	3.5

(a)

(b)

(c)

(d)

(e)

(f)

Figure 4. (a), (b) ADS layout of proposed FPR without and with metamaterial array; (c), (d) equivalent circuit of model proposed FPR without and with metamaterial array; (e), (f) front and rear view fabricated DSRR-based FPR.

the ADSlay out of the proposed FPR with and without the metamaterial array, while Figures 4(c) and (d) are representing their equivalent circuit models respectively. L_{TL} and C_{TL} are representing the characteristics of the FPR circuit where as R_{subs} is representing the substrate characteristics. The introduction of DSRR unit cell array is denoted by the combination of equivalent LC circuit with equivalent inductance L_{SRR} and equivalent capacitance, C_{SRR}. Moreover, a stray capacitance has been introduced in conjunction with the FPR circuit denoted by C_{stray}. This capacitance can be attributed to the gap between two consecutive unit cells. The descriptive overview of the circuit parameters is shown in Table 3. The proposed FPR has been designed and fabricated using an FR-4 substrate of relative permittivity $\varepsilon_r = 4.3$ and loss tangent $\delta = 0.025$ with substrate thickness $t = 1.6\,\mathrm{mm}$.

Advanced Design Software (ADS) and frequency domain solver of Computer Simulation Technology (CST) have been used for the simulation. The solver which is based on Finite Element Method (FEM), is specifically designed for electrically small and periodic structures as featured by the proposed DSRR-based FPR. The solver allows the electrical and magnetic field characteristics to be easily monitored for further optimization purpose. The fabricated DSRR-based FPR is shown in Figures 4(d) and 4(e). Measurements have been carried out with the help of Agilent's ENA E5071C network analyzer. Two ports of the proposed DSRR-based FPR are connected to the two ports of the network analyzer correspondingly while the other ports of FPR terminated with 50 Ohm termination.

Table 3. Parametric description of circuit in Figures 4(c) and 4(d).

Parameter	Value (mm)
L_{TL}	$10.5\,\mathrm{nH}$
C_{TL}	$2.3\,\mathrm{pF}$
R_{subs}	$2.5\,\Omega$
L_{SRR}	$12.5\,\mathrm{nH}$
C_{SRR}	$3\,\mathrm{pF}$
C_{stray}	$7.5\,\mathrm{pF}$

4. EXPERIMENTAL RESULTS AND DISCUSSIONS

The proposed DSRR metamaterial exhibited a wideband negative permittivity profile which is represented in Figure 5(a). For 1×1-unit cell, bandwidth with negative permittivity, is ranging from 0.5 to 4.35 GHz and 5.675 to 15 GHz which cover targeted resonances of the proposed FPR reflectometer. The same situation prevails in another arrays (namely 2×1, 3×3 and 4×5 array) where negative permittivity covers the whole region with a bandwidth extending from 0.5 GHz to 15 GHz (ENG bandwidth, $\mathrm{BW_{ENG}} = 187\%$). The reflection characteristics retrieved from EM simulation and circuit simulations are shown in Figure 5(b). It is found in the circuit simulation, the increasing value of C_{stray} has shifted the resonance frequency to the left, which indicates that if the unit cells are closely spaced, then it will shift the operating frequency of the FPR to the lower value. It can be seen that the FPR without the metamaterial array has a resonance frequency at 1.024 GHz as opposed to 1.176 GHz in the case of FPR with metamaterial. Moreover, the bandwidth less than $-10\,\mathrm{dB}$ reflection, $\mathrm{BW_{-10\,dB}}$ has been improved.
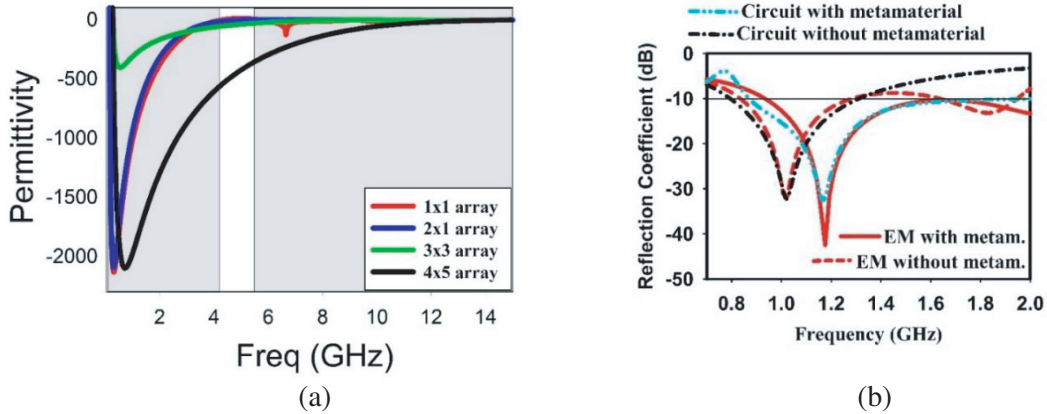
Figure 5. (a) Permittivity profile of different arrays of the metamaterial, (b) comparison of reflection coefficient characteristics in circuit and EM simulation for with and without metamaterial.

The simulated S-parameters of the proposed FPR with DSRR metamaterial has been paralleled with the measured results in Figure 6 while comprehensive overview is presented in Table 4 and Table 5. The $\mathrm{BW_{-10\,dB}}$ for the proposed reflectometer with DSRR metamaterial array extends from 0.9394 GHz until 2.19 GHz (79.79%) in simulation whereas it is covering 0.83 GHz to 1.28 GHz (42.65%) in the case of FPR without metamaterial. Therefore, there is an increase of 64.01% in the bandwidth of the proposed FPR. Meanwhile, the measured results are in agreement with the simulated results. The magnitude of the reflection coefficient (S_{11}), has also achieved a value near to zero in the resonance frequency as shown in Table 4.

In the simulation, the reflectometer has achieved a value of 0.00748 of the magnitude of S_{11} while the measured value is 0.0098. Moreover, the metamaterial array has improved the matching property of the junction by achieving a value of $-42.526\,\mathrm{dB}$ (simulation) and $-38.496\,\mathrm{dB}$ (measurement) while
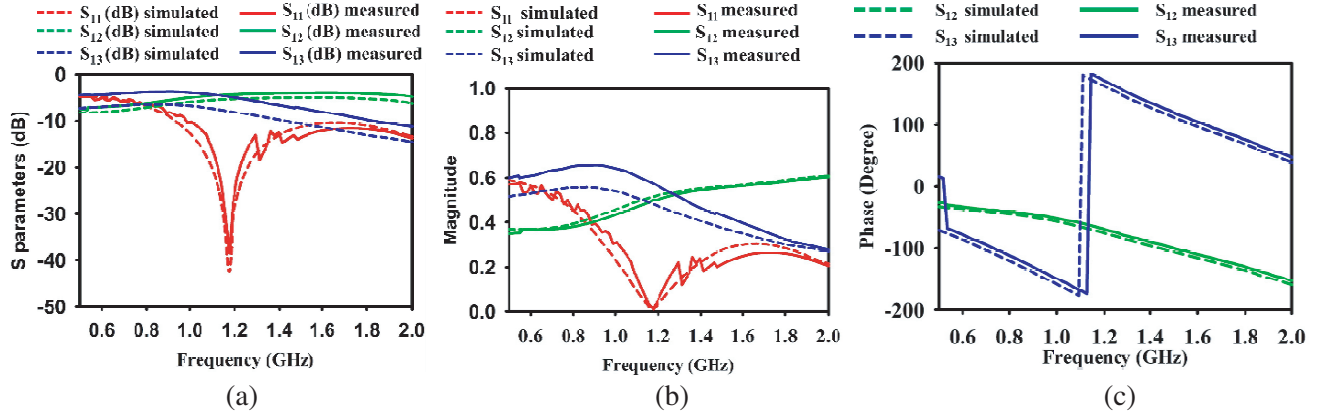
Figure 6. Measured and simulated results of FPR with metamaterial. (a) S-parameters (dB), (b) magnitude of S-parameters, (c) phase.

Table 4. Performance comparison of FPR with and without DSRR metamaterial.

Index	Description of the design category	$S_{11} < -10\,\text{dB}$		Resonance Frequency, F_r (GHz)	S_{11} (dB)	$\|S_{11}\|$	$\|S_{12}\|$ $(= \|S_{15}\|)$	$\|S_{13}\|$ $(= \|S_{14}\|)$
		Frequency (GHz)	Fractional Bandwidth $BW_{-10\,\text{dB}}$ (%)					
(a)	Theory		-	1	-	0	0.5	0.5
(b)	without DSRR	0.83–1.28	42.65%	1.024	−31.678	0.0261	0.4943	0.4701
(c)	with DSRR (Simul.)	0.9394–2.19	79.79%	1.176	−42.526	0.0075	0.5144	0.4503
(d)	with DSRR (Meas.)	0.991–2.2576	77.9%	1.176	−38.406	0.0098	0.501	0.4953
	$\|a-b\|$			-	-	0.0261	0.0047	0.0299
	$\|c-a\|$			-	-	0.0075	0.0144	0.0497
	$\|d-c\|$					0.0023	0.0134	0.045

**Table 5.** Phase characteristics proposed FPR with DSRR.

Index	Description of design category	Resonance Frequency, F_r (GHz)	Phase (°)		Phase Difference, $\Delta\varphi = \varphi_{S_{13}} - \varphi_{S_{14}}$
			$\varphi_{S_{12}}(= \varphi_{S_{15}})$	$\varphi_{S_{13}}(= \varphi_{S_{14}})$	
(a)	Theory	1	120	240	$\pm 120°(\mp 240°)$
(b)	without DSRR	1.024	−73.91	165.68	240.59
(c)	with DSRR (Simulation).	1.176	−73.37	166.68	240.05
(d)	with DSRR (Measurement).	1.176	−67.54	175.89	243.43
	$\|a-b\|$	-	-	-	0.59
	$\|c-a\|$	-	-	-	0.05
	$\|d-c\|$	-	-	-	0.38

theoretical parameters show only a value of $-31.678\,\text{dB}$. In addition, the bandwidth results shown in Table 4 also prove the advantage of the DSRR metamaterial array.

For the S-parameters, the measurement errors are varying from 0.0023 in S_{11} to 0.045 in S_{13}. The errors occurred in the measured results can be attributed to the losses in the RF cables and the fabrication errors. It can be seen from Table 5 that the phase differences for the proposed FPR with DSRR are around 240° which are very close to the theoretical values. The error between the

Table 6. Comparative overview of different ENG metamaterials.

Ref.	Epsilon Negative (ENG) band		Size of Unit cell
	Frequency (GHz)	Fractional bandwidth, BW_{ENG} (%)	
[21]	4.7–5.2	10	-
[23]	10.31–13.26	25.032	$0.17\lambda \times 0.11\lambda$
[24]	3.0–5.27	54.9	$0.09\lambda \times 0.04\lambda$
[25]	3.0–5.3	63.63	$0.06\lambda \times 0.06\lambda$
This work	0.5–15	187	$0.01\lambda \times 0.01\lambda$
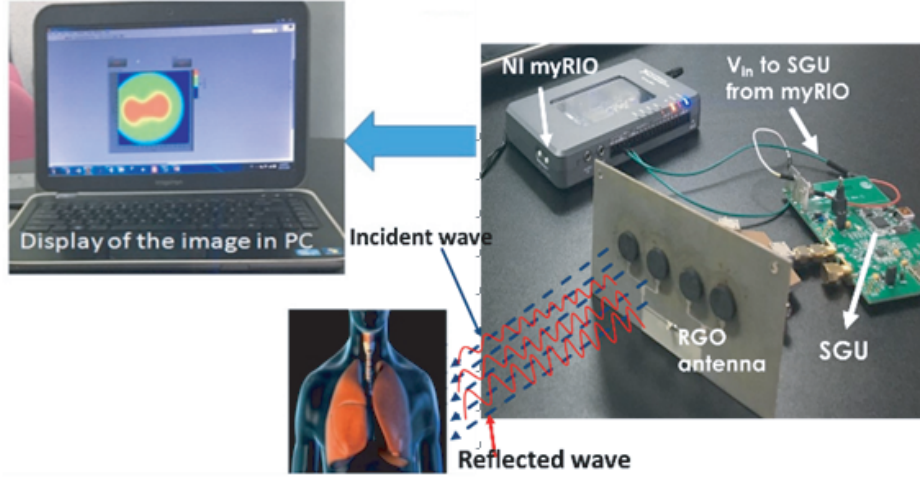
Figure 7. MWI system with proposed ENG DSRR metamaterial-based FPR.

measured and simulated phase difference is $0.38°$. In addition, to show the comparative superiority of the proposed DSRR metamaterial unit cell an overview is outlined in Table 6. It is observed that the proposed metamaterial atom has the highest epsilon negative fractional bandwidth BW_{ENG} of 187%. Figure 7 shows the MWI system consists of a signal generating unit (SGU) connected to port 4, whereas a reduced graphene oxide (RGO) antenna (designed in [29]) will be connected to port 5, as previously shown in Figure 1. The signal generating unit generates microwave pulses which are transmitted through the antenna. A very low amount of power is radiated towards the imaging body to avoid high radiation effect on the patient [30]. The backscattered signals is collected using the same antenna (following monostatic approach of radar-based MWI). Three diode power detectors are connected to other ports (port 1, port 2, and port 3). The detected signal power is converted into the digital form using an analog to digital converter (ADC). This is set as input to the reflection coefficient measurement algorithm (coded with LabVIEW according to the equations in [11]) embedded in myRIO. The excitation of the antenna is controlled according to the LabVIEW-based GUI. The antenna will be moved in different places around the imaging body. The complex reflection coefficient matrix $\Gamma(jk)$ is calculated corresponding to each frequency sample f and each antenna position $\overline{v_k}$ in $(f, k \in N)$. The generation of the image is followed according to DAS algorithm discussed in [5, 31]. For the sake of brevity, the image construction algorithm is not discussed here. Higher number of frequency samples will generate higher resolution image.

Figure 8 shows the regions of high intensity which are directly related to presence and location of the embedded tumor. When compared, it is evident that the proposed ENG DSRR metamaterial-based FPR with higher BW, provides better images than the FPR without metamaterial. In the reconstructed images, the tumor presence could hardly be detected (refer Figure 8(a)) while the integration of proposed FPR provides much better in resolution images (refer to Figure 8(b)). Thus the proposed
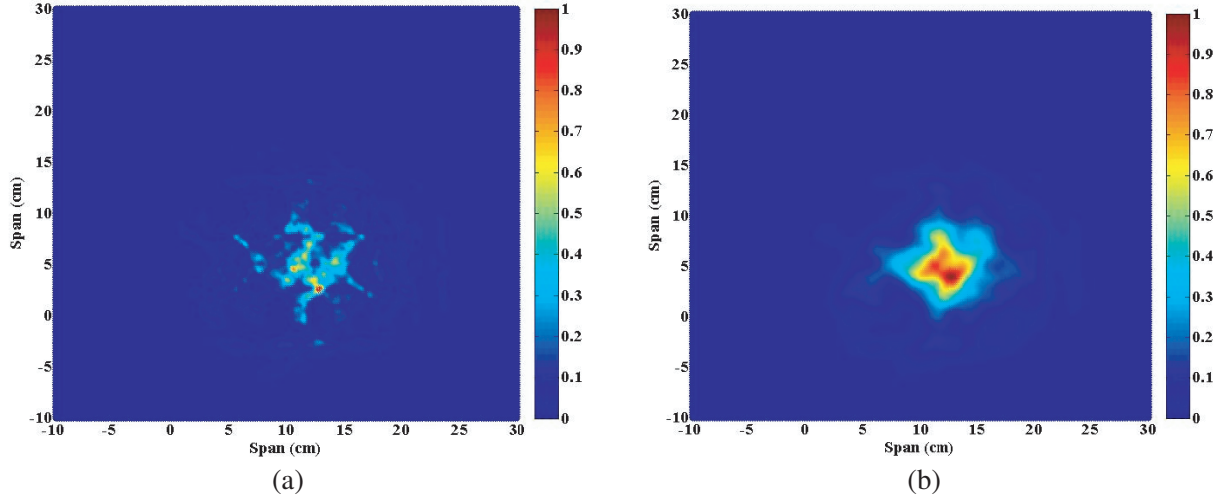
Figure 8. Initial bandwidth effect on the reconstructed image (a) lower bandwidth and (b) higher bandwidth.

ENG DSRR metamaterial-based reflectometer which has bandwidth of 77.9%, is capable of generating higher resolution image.

5. CONCLUSIONS

This paper proposes a symmetric five-port reflectometer (FPR) with UWB ENG DSRR metamaterial array in the ground plane. Proposed metamaterial array has covered an ENG fractional bandwidth, BW_{ENG} of 187%extending from 0.5 GHz to 15 GHz, which the highest reported bandwidth for DSRR based design. Moreover, proposed meta-atom can be used for other UWB applications as well. Proposed FPR with DSRR metamaterial array has covered a fractional bandwidth of $S_{11} < -10$ dB ($BW_{-10\,dB}$) of 79.79% (0.9394 GHz to 2.19 GHz). Moreover, other characteristics of FPR are also fulfilled by the design facilitating both higher penetration depth and higher spatial resolution for microwave imaging. Subsequently, proposed ENG DSRR in the rear part of the substrate has increased the bandwidth of the reflectometer by 64.01%. The operational characteristics of the proposed FPR is backed up using the comparison of EM simulation and circuit simulation following the proposition of equivalent circuit. Proposed metamaterial based FPR has proved its efficacious likelihood to be included in MWI system after being compared with the absence of metamaterial.

REFERENCES

1. Kurrant, D., J. Bourqui, C. Curtis, and E. Fear, "Evaluation of 3-D acquisition surfaces for radar-based microwave breast imaging," *IEEE Transactions on Antennas and Propagation*, Vol. 63, No. 11, 4910–4920, 2015.
2. Fear, E. C., J. Bourqui, C. Curtis, D. Mew, B. Docktor, and C. Romano, "Microwave breast imaging with a monostatic radar-based system: A study of application to patients," *IEEE Transactions on Microwave Theory and Techniques*, Vol. 61, No. 5, 2119–2128, 2013.

3. Fear, E. C., P. M. Meaney, and M. A. Stuchly, "Microwaves for breast cancer detection," *IEEE Potentials*, Vol. 22, No. 1, 12, 2003.

4. Zwick, T., L. Zwirello, M. Jalilvand, and X. Li, "Ultra wideband compact near-field imaging system for breast cancer detection," *IET Microwaves, Antennas & Propagation*, Vol. 9, No. 10, 1009–1014, 2015.

5. Ireland, D. and M. Bialkowski, "Microwave head imaging for stroke detection," *Progress In Electromagnetics Research M*, Vol. 21, 163–175, 2011.

6. Mohammed, B. J., A. M. Abbosh, D. Ireland, and M. E. Bialkowski, "Compact wideband antenna for microwave imaging of brain," *Progress In Electromagnetics Research C*, Vol. 27, 27–39, 2012.

7. Mobashsher, A. T. and A. M. Abbosh, "Performance of directional and omnidirectional antennas in wideband head imaging," *IEEE Antennas and Wireless Propagation Letters*, Vol. 15, 1618–1621, 2016.

8. Abbosh, A. M., A. Zamani, and A. T. Mobashsher, "Real-time frequency-based multistatic microwave imaging for medical applications (Invited)," *2015 IEEE MTT-S International Microwave Workshop Series on RF and Wireless Technologies for Biomedical and Healthcare Applications, IMWS-BIO 2015 — Proceedings*, 127–128, 2015.

9. Guo, L. and A. M. Abbosh, "Compressive sensing for stroke detection in microwave-based head imaging," *IEEE Antennas and Propagation Society, AP-S International Symposium (Digest)*, 1911–1912, 2014.

10. Lee, C. Y., K. Y. You, Z. Abbas, K. Y. Lee, Y. S. Lee, and E. M. Cheng, "S-band five-port ring reflectometer-probe system for in vitro breast tumor detection," *International Journal of RF and Microwave Computer-Aided Engineering*, Vol. 28, No. 3, e21198, Mar. 2018.

11. Yee, L. K., Z. Abbas, M. A. Jusoh, Y. K. Yeow, and C. E. Meng, "Determination of moisture content in oil palm fruits using a five-port reflectometer," *Sensors*, Vol. 11, No. 4, 4073–4085, Apr. 2011.

12. Kim, D. I., K. Araki, and Y. Naito, "Properties of the symmetrical circuit and its broad-band five-port design," *IEEE Transactions on Microwave Theory and Techniques*, Vol. 32, No. 1, 51–57, Jan. 1984.

13. Yeo, S. P. and F. C. Choong, "Matched symmetrical five-port microstrip coupler," *IEEE Transactions on Microwave Theory and Techniques*, Vol. 49, No. 8, 1498–1500, 2001.

14. Hansson, E. R. B. and G. P. Riblet, "An ideal six-port network consisting of a matched reciprocal lossless five-port and a perfect directional coupler," *IEEE Transactions on Microwave Theory and Techniques*, Vol. 31, No. 3, 284–288, 1983.

15. Hansson, E. R. B. and G. P. Riblet, "The matched symmetrical five-port junction as the essential part of an ideal six-port network," *11th European Microwave Conference, 1981*, 501–506, 1981.

16. Belfort, A. J. and A. L. Cullen, "First-order theory of the five-port symmetrical star junction," *Electronics. Letters*, Vol. 18, No. 19, 841, 1982.

17. Baharuddin, S. A., et al., "Development of five port reflectometer for reflection based sensing system," *AIP Conference Proceedings*, Vol. 1808, No. 1, 20011, 2017.

18. Al-Bawri, S. S., M. F. Jamlos, S. Z. Ibrahim, and S. A. Aljunid, "Compact multilayer wideband symmetric five-port reflectometer," *Microwave and Optical Technology Letters*, Vol. 59, No. 4, 802–805, Apr. 2017.

19. Lee, C. Y., K. Y. You, T. S. Tan, Y. L. Then, Y. S. Lee, L. Zahid, W. L. Lim, and C. H. Lee, "Enhanced five-port ring circuit reflectometer for synthetic breast tissue dielectric determination," *Progress In Electromagnetics Research C*, Vol. 69, 83–95, 2016.

20. Hossain, T. M., M. A. F. Jamlos, M. A. F. Jamlos, P. J. Soh, M. I. Islam, and R. Khan, "Modified H-shaped DNG metamaterial for multiband microwave application," *Applied Physics A*, Vol. 124, No. 2, 183, 2018.

21. Smith, D. R., et al., "Composite medium with simultaneously negative permeability and permittivity," *Physics Review Letters*, Vol. 84, No. 18, 4184–4187, May 2000.

22. Rusni, I. M., A. Ismail, A. R. H. Alhawari, M. N. Hamidon, and N. A. Yusof, "An aligned-gap and

centered-gap rectangular multiple split ring resonator for dielectric sensing applications," *Sensors (Basel, Switzerland)*, Vol. 14, No. 7, 13134–13148, 2014.

23. Islam, M. T. M. M., M. T. M. M. Islam, M. Samsuzzaman, M. R. I. Faruque, N. Misran, and M. F. Mansor, "A miniaturized antenna with negative index metamaterial based on modified SRR and CLS unit cell for UWB microwave imaging applications," *Materials (Basel)*, Vol. 8, No. 2, 392–407, 2015.

24. Islam, M. T., M. M. Islam, M. Samsuzzaman, M. R. Iqbal Faruque, and N. Misran, "A negative index metamaterial-inspired UWB antenna with an integration of complementary SRR and CLS unit cells for microwave imaging sensor applications," *Sensors (Basel, Switzerland)*, Vol. 15, No. 5, 11601–11627, 2015.

25. Alhawari, A. R. H., A. Ismail, M. A. Mahdi, and R. S. A. R. Abdullah, "Miniaturized ultra-wideband antenna using microstrip negative index metamaterial," *Electromagnetics*, Vol. 31, No. 6, 404–418, 2011.

26. Nordin, M. A. W., M. T. Islam, and N. Misran, "Design of a compact ultrawideband metamaterial antenna based on the modified split-ring resonator and capacitively loaded strips unit cell," *Progress In Electromagnetics Research*, Vol. 136, 157–173, 2013.

27. Hansson, E. R. B. and G. P. Riblet, "An ideal six-port network consisting of a matched reciprocal lossless five-port and a perfect directional coupler," *IEEE Transactions on Microwave Theory and Techniques*, Vol. 31, No. 3, 284–288, 1983.

28. Pozar, D., *Microwave Engineering*, 3rd Edition, 2004.

29. Aminudin, M., J. Abdul, H. Ismail, and M. Faizal, "Hybrid graphene-copper UWB array sensor for brain tumor detection via scattering parameters in microwave detection system," *Applied Physics A*, 1–7, 2017.

30. Mobashsher, A. T., A. M. Abbosh, and Y. Wang, "Microwave system to detect traumatic brain injuries using compact unidirectional antenna and wideband transceiver with verification on realistic head phantom," *IEEE Transactions on Microwave Theory and Techniques*, Vol. 62, No. 9, 1826–1836, 2014.

31. Fear, E. C., X. Li, S. C. Hagness, and M. A. Stuchly, "Confocal microwave imaging for breast cancer detection: Localization of tumors in three dimensions," *IEEE Transactions on Biomedical Engineering*, Vol. 49, No. 8, 812–822, 2002.